Research Article | Vol. 11, No. 2 / 1 February 2020 / Biomedical Optics Express 1092
Biomedical Optics EXPRESS

Optical coherence tomography for evaluating capillary waves in blood and plasma

Hsiao-Chuan Liu,[1,*] Piotr Kijanka,[1,2] and Matthew W. Urban[1,3]

[1]*Department of Radiology, Mayo Clinic, 200 First St SW, Rochester, MN 55905, USA*
[2]*Department of Robotics and Mechatronics, AGH University of Science and Technology, Al. Mickiewicza 30, Krakow 30-059, Poland*
[3]*Department of Physiology and Biomedical Engineering, Mayo Clinic, 200 First St SW, Rochester, MN 55905, USA*
[*]*liu.hsiao-chuan@mayo.edu*

Abstract: Capillary waves are associated with fluid mechanical properties. Optical coherence tomography (OCT) has previously been used to determine the viscoelasticity of soft tissues or cornea. Here we report that OCT was able to evaluate phase velocities of capillary waves in fluids. The capillary waves of water, porcine whole blood and plasma on the interfacial surface, air-fluid in this case, are discussed in theory, and phase velocities of capillary waves were estimated by both our OCT experiments and theoretical calculations. Our experiments revealed highly comparable results with theoretical calculations. We concluded that OCT would be a promising tool to evaluate phase velocities of capillary waves in fluids. The methods described in this study could be applied to determine surface tensions and viscosities of fluids for differentiating hematological diseases in the future potential biological applications.

1. Introduction

Capillary waves are a surface wave propagating along the phase boundary of a fluid. Phase velocities of capillary waves on fluids are related to fluid depth, gravity, fluid density, surface tension and viscosities [1,2]. Understanding fluid mechanical properties are important, such as for blood. Blood is a specialized body fluid that can transport oxygen and nutrients to the cells. Its thicker consistency, deriving from suspended platelets, erythrocytes, leukocytes, plasma and proteins, with non-Newtonian characteristics make the fluid complex [3,4]. The viscosity of blood and plasma are important parameters in clinical practice. Blood viscosity is mainly determined by the concentration of hematocrit [5]; however, the larger aggregation of red blood cells (RBCs), deformability of RBCs and plasma fibrinogen concentration also contribute to an increase in blood viscosity [6]. Disorders of blood viscosity are significantly associated with the progression of coronary heart disease [7,8], peripheral artery diseases [9] stroke [10] and hyperviscosity syndromes [11,12] which occur in polycythaemia, leukemia, sickle cell diseases and paraproteinaemias [6]. Also, one of the hyperviscosity syndromes called macroglobulinemia can be diagnosed because the molecular weight of protein IgMs is five times higher than normal so that the viscosity is increased [13]. According to Stokes theory [1], phase velocities of capillary waves are mainly associated with viscosities and surface tensions of fluids; therefore, evaluating phase velocities of capillary waves of fluids are essential.

Two fundamental techniques in clinics for providing an assessment of viscosities in blood are: thromboelastgraphy (TEG) and rotation thromboelastography (ROTEM), which have been widely used in liver transplantation, hemophilia, trauma, obstetrics and cardiac surgery [14]. The TEG output depictions can explain various kinetics in coagulopathic states such as hemophilia, fibrinolysis or thrombocytopenia. However, a lack of standardized methodologies, relatively high coefficient of variation and poor repeatability need to be considered [15,16]. Recently,

#382819 https://doi.org/10.1364/BOE.382819
Journal © 2020 Received 8 Nov 2019; revised 13 Jan 2020; accepted 14 Jan 2020; published 24 Jan 2020

Biomedical Optics EXPRESS

microfluidic devices have been developed to measure viscosity of blood [17,18] due to high accuracy, customized functions in fluidic networks, such as twin-shaped microfluidic device, stabilization in the microfluidic device and sensorless detection [18,19]. However, microchannel network design must be precisely designed to achieve the desired features [19]. Although the soft lithography based on polydimethylsiloxane (PDMS) is widespread used to fabricate devices, it is ill-suited for mass production [20]. On the other hand, to perfectly control fluids inside microchannels, specific systems might be required, such as pinch valves, peristaltic pump or pressure controllers [18].

Optical coherence elastography (OCE), using the optical coherence tomography (OCT) system structure, has been maturely used to evaluate mechanical properties of tissues [21–25]. OCE has become a popular technology used to investigate mechanical properties of small tissues during the last decade due to a number of advantages, including being noncontact, and having high spatial resolution and sensitivity to the topology of a surface [24,26]. Previous studies have demonstrated that OCE has the capability to characterize mechanical properties of skin [27], chicken breast [28], rat tumor tissue [29], prostate cancer [30], carotid artery [31] and especially cornea, retinal and lens in the eye [24,32–38]. The full-field OCT (FF-OCT) was proposed to follow shear wave propagation and assess the stiffness of gel phantoms [39]. Recently, some articles demonstrated that OCE [16] and optical-based methods, such as magnetomotive OCE [40] or laser speckle rheology (LSR) method [41], are capable of assessing the mechanical properties of blood clots. However, the study of using OCE to investigate the rheology properties of blood and plasma in the liquid phase has not been reported.

In this article we propose that OCT would be a promising tool to estimate phase velocities of capillary waves induced with acoustic radiation force in fluids. In theory, phase velocities of capillary waves are associated with fluid depth, gravity, surface tension, viscosity, and fluid density [1,2]. Once the wavelength is smaller than 1.73 cm in water, waves will enter the capillary regime and surface tension dominates wave velocities and gravity can be negligible [1,42]. Acoustic radiation forces were exerted on the fluid-air interface to generate a capillary wave, which can be imaged similar to watching the effects of a stone thrown in a pond to make ripples, if the depth of the water is smaller than half a wavelength [43]. The OCT working with a 10 kHz scan rate was used to record capillary waves of water, porcine whole blood and plasma. Phase velocities of capillary waves from theoretical calculations were compared with our experimental results.

2. Materials and methods

2.1. Blood preparation

The blood and plasma preparation is followed by a standard protocol [3]. The porcine whole blood with K3-EDTA anticoagulant was purchased from LAMPIRE Biological Laboratories, Inc. (Pipersville, PA, USA). A 40 ml whole blood sample was taken by using a micropipette and immediately transferred to 8 individual 6 ml sterile polystyrene tubes (Becton Dickinson, Lincoln Park, NJ, USA). In each polystyrene tube 5 ml of whole blood was distributed and then were centrifuged (VWR Clinical 200, Radnor, PA, USA) for 12 min at 1440 g to separate the cellular components of whole blood, including RBCs, white blood cells and platelets from plasma. After centrifugation, the plasma in the polystyrene tubes was transferred to a 100×15 mm sterile polystyrene Petri dish (Bioplast Manufacturing, Bristol, PA, USA) to make the depth of fluids 3 mm. Sufficient plasma residual volume was left in the polystyrene tubes during the pipetting to avoid disturbing the buffy coat and to insure the quality of the plasma. For the whole blood experiment, the 20 ml of whole blood was taken using the micropipette and transferred to the Petri dish for the experiment. The temperature of the blood and plasma was 23°C (room temperature).

Biomedical Optics EXPRESS

2.2. System structure of acoustic radiation force optical coherence tomography (ARF-OCT)

The system was composed of a spectral domain optical coherence tomography (SD-OCT) scanner, a focused ultrasound transducer, function generators and radiofrequency (RF) amplifier, illustrated in Fig. 1(a). For the optical scanner, the 1300 nm central wavelength superluminescent diode (SLD) light source with the high power and brightness is used to generate the low coherence broadband source in the SD-OCT system (TEL320C1, Thorlabs Inc., Newton, NJ, USA). The low coherence broadband source is split into two beams: a reference beam directed towards a stationary reference mirror and a sample beam directed towards samples. The sample beam is routed over two galvanometer actuated mirrors to allow for scanning in two axes. The scan objective (OCT-LK3, Thorlabs Inc., Newton, NJ, USA) then focuses the beam from the sample and provide 13 µm lateral resolution and 3.6 mm of imaging depth in air within 10 mm x 10 mm field of view (FOV). Back-scattered and back-reflected light is collected by the scan objective and travels back to the fiber. The back-reflected and back-scattered light from samples and retro-reflected light from the reference mirror are recombined and the spectrometers are utilized to form a spectral interferogram. The bandwidth of the light source is 236.8 nm and the optical axial resolution is 5.5 µm in air, provided by Thorlabs Inc. An A-scan signal in the OCT system is stored as a stream of 32-bit (single-precision) unsigned floating point data in little-endian byte order. Each pixel includes a real value and an imaginary value from which magnitude and phase values can be calculated. The Fast Fourier Transform (FFT) is utilized to form the A-scan in the OCT system. In the study, only magnitude signals were used to detect the small perturbations of waves on the surface of liquids.

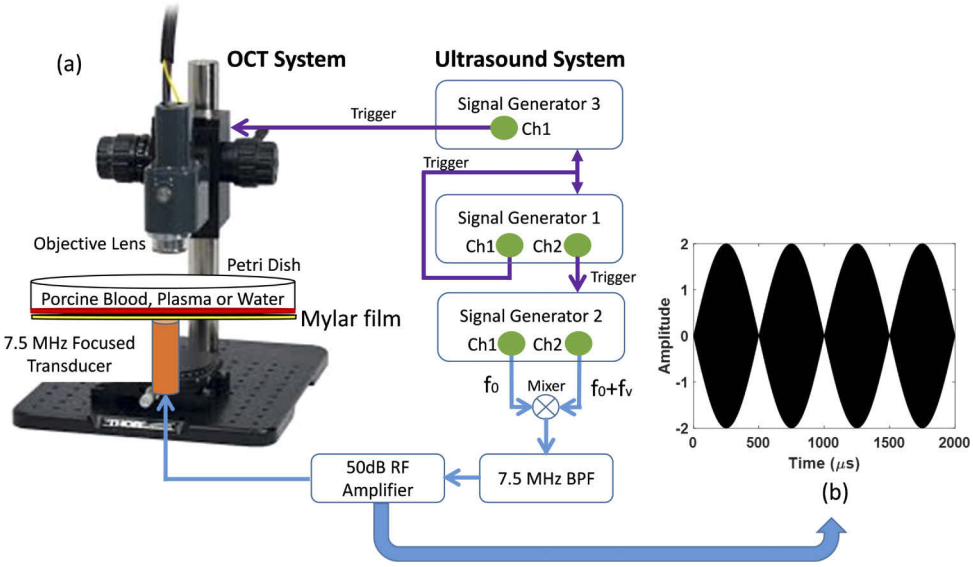

Fig. 1. Illustration of the system structure of acoustic radiation forced OCT. (a) left side displays our SD-OCT scanner and right side is the ultrasound system to generate acoustic radiation force. Three function generators were used to manage all signals for the whole system including ultrasound excitation signals (blue lines) and trigger signals for synchronizing all instruments (purple lines). The BPF stands for band pass filter and RF is radio frequency. (b) Illustration of a double sideband suppressed carrier amplitude modulation (DSB-SC AM) signal in 2 kHz modulation during 2 ms.

Biomedical Optics EXPRESS

To capture the propagation of capillary waves in whole blood and plasma, the M-B scan mode was used to track dynamic processes in the space-time domain [44]. The customized acquisition in two dimensions (2D) was set to obtain data at 100 lateral step sizes with 0.1 mm interval within a 10 mm field-of-view. For each M-scan, the OCT repeats 500 times at 10 kHz scan rate; therefore, the scan time for each B-scan takes 5 seconds in 2D acquisition The three-dimensional (3D) OCT image consisted of repeating the 2D scans 100 times with 0.1 mm scanning step in both the lateral and elevation direction. This customized acquisition was developed by using C++ with a SpectralRadar software development kit (SDK) 4.4 version provided by Thorlabs in Microsoft Visual Studio 2019 development environment (Microsoft, Redmond, WA).

A focused transducer with a center frequency of 7.5 MHz (ISO703HR, Valpey-Fisher, Hopkinton, MA, USA) with burst sinusoid signals of 15,000 cycles was used to produce the acoustic radiation force exerted on the surface of fluids. The bottom of the Petri dish was replaced by Mylar film with 100 µm thickness; therefore, the acoustic power will only be weakly attenuated. The focal distance and f-number was 11.84 mm by pulse-echo response and of 1.07 by the definition of the focal distance divided by the aperture size (11 mm) were obtained, respectively. In our experiments, the capillary waves are able to be generated as the acoustic radiation force were positioned certain small deviations from the surface of fluids if a highly focused transducer is used. With the highly focused transducer, a lateral focal size can be calculated by the equation: $2.44 \times f\#\times$ and is 514.84 µm in the study [45]. Therefore, the focal size is small enough, compared with the FOV in OCT, to generate capillary waves even though the surface of fluids is positioned slightly close to transducer (in the near field).

Our previous research demonstrates that double sideband suppressed carrier amplitude modulation (DSB-SC AM) technique is a useful tool for characterizing viscoelastic properties of a tissue mimicking phantom material [46]. Therefore, DSB-SC AM technique was adopted in the study to create the capillary waves of whole blood and plasma. Consider a sine wave signal *x(t)* with center frequency f_c and amplitude A given by

$$x(t) = Asin(2\pi f_c t) \tag{1}$$

Let *y(t)* represent a base signal with added modulation frequency.

$$y(t) = kAsin(2\pi(f_c + f_m)t + \theta) \tag{2}$$

where k is amplitude sensitivity that can be varied from 0 to 1, f_m is modulation frequency and θ is phase shift. The AM modulated signal $m(t)$ can be written as

$$m(t) = Asin(2\pi f_c t) + kAsin(2\pi(f_c + f_m)t + \theta) \tag{3}$$

In the study, we selected $k = 1$ and $\theta = 180°$ to represent 100% modulation. Using trigonometric identities, *m(t)* can be reformed as follows.

$$m(t) = Asin(2\pi f_c t) - Asin(2\pi(f_c + f_m)t) \tag{4}$$

The f_m was set as 2 kHz during 2 ms to generate a 4-cycle modulation signal. Figure 1(b) is a simulation result based on Eq. (4). The ultrasound AM modulation techniques details are discussed in previous literature [46].

Three function generators were employed to manage the whole system. Capillary waves on water, whole blood, and plasma were generated by modulated acoustic radiation force provided by a function generator (33250A, Agilent, Santa Clara, CA, USA) triggered by signal generator 1 [Fig. 1(a)] and was amplified in 50 dB by a radiofrequency (RF) power amplifier (240L, Electronics and Innovation, LTD, Rochester, NY, USA) to drive the transducer. The second function generator (33500B, Keysight, Santa Rosa, CA, USA) was set as a 20 Hz square wave as a

Biomedical Optics EXPRESS

master trigger for excitation signal and the whole system to synchronize all the timing. The third function generator controlled the OCT timing. In our experiment, the OCT was acquiring 500 lines at each location with a 10 kHz scan rate. Therefore, the necessary time to complete a whole scan at each location was 50 ms, which is a 20 Hz measurement rate. A 2 ms excitation signal repeated every 50 ms was transmitted to excite the fluids to generate capillary waves and the OCT immediately started scanning at a 10 kHz rate once the excitation signals were transmitted. Twenty cases were collected in water, whole blood and plasma for each type fluid.

2.3. Capillary waves on water, whole blood and plasma

A capillary wave is a surface wave propagating along the phase boundary of a fluid and it is produced by a small stress exerted on the interface between fluid and air. An acoustic radiation force exerted on the surface of fluids is similar to a droplet falling in a puddle due to a small aperture size. If a water-air free surface is considered with small amplitude waves and fluids that have a uniform depth, are imcompressible and irrotational, then the wave propagation in the x-direction with phase velocity C_p and dispersion relation are given by following equation based on Airy wave theory [43].

$$C_p = \frac{\omega}{k} = \sqrt{\frac{1-\left(\frac{\rho'}{\rho}\right)}{1+\left(\frac{\rho'}{\rho}\right)}\left(\frac{g}{k}+\frac{\sigma k}{\Delta\rho}\right)\tanh(kh)} \tag{5}$$

$$\omega^2 = \frac{1-\left(\frac{\rho'}{\rho}\right)}{1+\left(\frac{\rho'}{\rho}\right)}\left(gk+\frac{\sigma k^3}{\Delta\rho}\right)\tanh(kh) \tag{6}$$

where g is gravity, k is the wavenumber ($2\pi/\lambda$), h is the depth of the fluid, ω is the angular frequency, σ is surface tension, and ρ and ρ' are the mass density of water and air, respectively. The regime between gravity and capillary waves can be characterized by the Eötvös (Eo) number (or called Bond number) composed with capillary forces (surface tension), gravitational forces, wavelength and mass density.

$$Eo = \frac{\Delta\rho g}{\sigma k^2} = \frac{\Delta\rho g\lambda^2}{\sigma(2\pi)^2} = \left(\frac{\lambda}{2\pi\lambda_{capillary}}\right)^2 \tag{7}$$

where $\lambda_{capillary} = \sqrt{\frac{\sigma}{\Delta\rho g}}$ is the capillary length. The Eo number will be close to 1 if λ is equal to $2\pi\lambda_{capillary}$. For the water-air interface, the surface tension is 74 mN/m, the mass density of water is 1000 kg/m^3, the mass density of air is 1.2 kg/m^3, and gravity is 9.81 m/s^2. The critical wavelength λ_c is found to be 17.25 mm and the associated minimum phase velocity $C_{p(min)}$ is 0.231 m/s if the depth of the water h is assumed to be 5 mm. The minimum phase velocity $C_{p(min)}$ and the critical wavelength λ_c based on the Eqs. (5) and (7) were illustrated in Fig. 2(a) with the red dot. If λ is much larger than $2\pi\lambda_{capillary}$, which means that Eo number is larger than 1, then the wave in this condition is named a *gravity wave* and the surface tension can be neglected. On the contrary, the wave is defined as a *capillary wave* if λ is much smaller than $2\pi\lambda_{capillary}$ (Eo number << 1) and gravity can be neglected in this case.

Various water depths generate different properties of waves on the surface for both gravity waves and capillary waves. In general, the water depth h can be classified into three regimes: deep water, shallow water and intermediate water. The deep water and shallow water are defined as $h > 0.5\lambda$ and $h < 0.05\lambda$, respectively [43]. In the gravity wave regime, the phase velocity C_{pGra}

Biomedical Optics EXPRESS

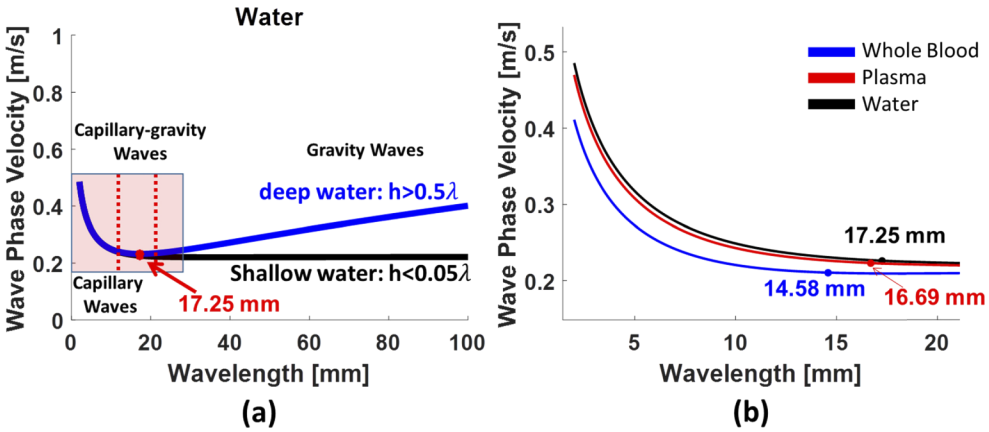

Fig. 2. (a) The theoretical calculations of capillary waves and gravity waves in deep water and shallow water. The critical wavelength λ_c is found to be 17.25 mm and the associated minimum phase velocity $C_{p(min)}$ is 0.231 m/s. The blue line and black line are waves in deep water and in shallow water, respectively. (b) The critical wavelengths λ_c in three fluids, water, plasma and whole blood, were calculated.

can be modified as follows based on Eq. (5).

$$C_{pGra} = \sqrt{\frac{g}{k}\tanh(kh)} \tag{8}$$

In this regime, $\tanh(kh)$ is close to 1 as $h > 0.5\lambda$ for deep water and $\tanh(kh)$ is close to kh if h is smaller than 0.05λ for shallow water, and the phase velocity in deep water and shallow water are given by

$$C_{pGra\_deep} = \sqrt{\frac{g}{k}}\ h > 0.5\lambda\ or\ kh > \pi \tag{9}$$

$$C_{pGra\_shallow} = \sqrt{gh}\ h < 0.05\lambda\ or\ kh < 0.1\pi \tag{10}$$

The phase velocity of gravity waves in deep water C_{pGra_deep} will be largely influenced by wavelength and longer waves will travel faster than shorter waves, presented in Fig. 2(a) with the blue line. For the phase velocity of gravity waves in shallow water $C_{pGra\_shallow}$, the speed is only dependent of the depth of water; therefore, wavelengths travel at the same speed and there is no dispersion, illustrated in Fig. 2(a) with black line. The group velocity of a gravity wave in deep water C_{gGrp_deep} is given by

$$C_{gGrp\_deep} = \frac{d\omega}{dk} = \frac{d\sqrt{gk}}{dk} = 0.5C_{pGra\_deep} \tag{11}$$

The group velocity of gravity waves in deep water is always slower than phase velocity.

On the other hand, in the capillary wave regime, the phase velocity C_{pCap} is given by

$$C_{pCap} = \sqrt{\frac{1-\left(\frac{\rho'}{\rho}\right)}{1+\left(\frac{\rho'}{\rho}\right)}\left(\frac{\sigma k}{\Delta\rho}\right)\tanh(kh)} \tag{12}$$

In this capillary regime, the water depth can also be classified into deep water as $h > 0.5\lambda$ and shallow water if $h < 0.05\ \lambda$. The phase velocity in deep water and shallow water can be written

Biomedical Optics EXPRESS

as follows.

$$C_{pCap\_deep} = \sqrt{\frac{1-\left(\frac{\rho'}{\rho}\right)}{1+\left(\frac{\rho'}{\rho}\right)}\left(\frac{\sigma k}{\Delta\rho}\right)} \; h > 0.5\lambda \; or \; kh > \pi \tag{13}$$

$$C_{pCap\_shallow} = \sqrt{\frac{1-\left(\frac{\rho'}{\rho}\right)}{1+\left(\frac{\rho'}{\rho}\right)}\left(\frac{\sigma hk^2}{\Delta\rho}\right)} \; h < 0.05\lambda \; or \; kh < 0.1\pi \tag{14}$$

The phase velocity of capillary waves in deep water C_{pCap_deep} will be largely influenced by surface tension and shorter waves will travel faster than longer waves, presented in Fig. 2(a) with the blue line in the pink window. For the phase velocity of capillary waves in shallow water $C_{pCap\_shallow}$, wavelength and water depth will considerably dominate phase velocity and the phase velocity will travel even slower than those in deep water at the same wavelength. Moreover, the Van der Waals force will also be considered [42]. Capillary waves in shallow water were not the case in this study because the depth h of water will reach to scales of a few hundred micrometers. The group velocity of capillary waves in deep water C_{gCap_deep} can be written as

$$C_{gCap\_deep} = \frac{d\omega}{dk} = \frac{d}{dk}\frac{1-\left(\frac{\rho'}{\rho}\right)}{1+\left(\frac{\rho'}{\rho}\right)}\left(\frac{\sigma k^3}{\Delta\rho}\right) = \frac{3}{2}C_{pCap\_deep} \tag{15}$$

The group velocity of capillary waves in deep water is always faster than phase velocity. In addition, for the case that h is between 0.5λ and 20λ is called intermediate water and the wave is defined as capillary-gravity waves. In this case, all terms in Eq. (5) need to be considered to evaluate phase velocities.

The minimum phase velocity and associated wavelength in whole blood and plasma can be estimated according to the Eq. (5). Previous literature reported that the mass density and surface tension of human whole blood and plasma is similar with porcine whole blood and plasma [47]. In the study, the mass density is assumed to be 1060 kg/m^3 in whole blood and 1025 kg/m^3 in plasma [48,49]. The surface tension of whole blood and plasma is assumed to be 56 mN/m and 71 mN/m, respectively [2,50]. The depth h of whole blood and plasma was approximately 3-4 mm in our experiment. According to the Eq. (5), the minimum phase velocity and capillary wavelength were 0.206 m/s and 14.58 mm in whole blood, respectively, and 0.222 m/s and 16.69 mm in whole blood, respectively. The red line and blue line in Fig. 2(b) demonstrated the minimum phase velocity in whole blood and plasma. Our experimental results demonstrate that the wavelengths were smaller than the critical wavelength in the most cases and deep h of fluids was 3 mm in the experiment; therefore, the wave is capillary wave in deep water regime in the most of case. For certain wavelengths which range between 0.5λ and 20λ, the capillary-gravity waves were considered.

2.4. Signal processing of capillary waves

In the study, only magnitude signals were used to detect the small perturbations of waves on the surface of liquids because a capillary wave is a surface wave propagating along the phase boundary of a fluid. The 2D acquisition is composed of m by n matrix, where m is imaging depth and n is the number in M-scan multiplied by B-scan, which is 500,000 in the study. Later, the m by n matrix was reformed to m by k by t matrix, where k is the number in B-scan and t is the number in M-scan. A median filter was employed to remove noise from a two-dimensional wave motion image before autocorrelation was performed. The data in each column of the wave motion image was upsampled by 5 times by spline interpolation. The autocorrelation of magnitude A-scan data

Biomedical Optics EXPRESS

was used to estimate the displacement amplitude of capillary waves on the liquid surface [51,52]. After the autocorrelation calculation, the wave amplitudes were subtracted by their mean value to make the base line of wave motions to be zero and the wave motion images with time factor and propagation distance were reconstructed. A two-dimensional Fourier transform (2D-FT) with size 5120 × 5120 points was used to decompose multiple frequencies from two-dimensional (2D) wave motion images to obtain a wavenumber-frequency representation (k-space) for dispersion analysis [52,53].

3. Results and discussion

According to Eq. (5), the velocity of capillary waves varies with wavelength. The depth of water was 3 mm in the experiment and the critical wavelength λ_c was found to be 17.25 mm and the associated minimum phase velocity $C_{p(min)}$ was 0.231 m/s, based on Eqs. (5) and (7). The capillary waves on the water surface can be generated by acoustic radiation forces and clearly observed by using 3D-OCT images, presented in Fig. 3. We focus on a single wavelength on the 3D-OCT images at 15 ms [Fig. 3(a)], the travel distance was 5.4 mm (white arrow); therefore, the wave velocity is approximately 0.36 m/s. On the other hand, the wavelength at this time point was 4.1 mm (orange arrow) so that the capillary wave is in the deep water regime (h>0.5λ). According to the Eq. (12), the capillary phase velocity was 0.3459 m/s [black dot on Fig. 3(d)], which is close to our experimental results. We also examined wavelengths at different time points, 20 ms and 25 ms illustrated in Fig. 3(b) and Fig. 3(c), respectively. At 20 ms, the travel distance was 6.5 mm and the wavelength was increased to 4.7 mm. The C_{pCap_deep} in the experimental and theoretical results were 0.325 m/s [Fig. 3(b)] and 0.3257 m/s [red dot on Fig. 3(c)], respectively. At 25 ms, we obtained 0.32 m/s [Fig. 3(c)] from the experiment and 0.3173 m/s [blue dot on Fig. 3(d)] based on the theory, respectively. Moreover, Fig. 3(a)–3(c) clearly displayed that the shorter waves travels faster than longer waves in capillary waves, which is reasonable because wavenumber k has a positive relation with C_{pCap_deep} according to Eq. (13). The precision of this measurement is governed by the scanning step of our scans which was 0.1 mm in this study. Finer scanning steps could be used for fluids with higher wave velocities. A video of 3D capillary wave propagation on water displayed longer waves and shorter waves (see Visualization 1). According to Eq. (15), group velocities of capillary waves C_{gCap_deep} in deep water are 1.5 times faster than phase velocities. We report that OCT would be a promising tool to evaluate capillary waves with small fluctuations on the water-air interfacial surface.

In the experiments, wavelength changes cannot be completely recorded due to the limitation of small field of view (FOV) of the OCT (10 mm by 10 mm) and phase velocities is a function of wavelengths. Therefore, a two-dimensional Fourier transform (2D-FT) was used to decompose multiple frequencies from two-dimensional (2D) wave motion images to obtain a wavenumber-frequency representation (k-space) [53]. The 2D wave motion image at 5 mm position on y-axis of OCT was shown in Fig. 4(a). The two capillary waves, longer waves and shorter waves were observed. Due to different frequency components in longer and shorter waves, two regions-of-interest (ROIs) are discussed separately: white dashed quadrilateral for longer waves and black dashed quadrilateral for shorter waves [Fig. 4(a)]. Because shorter waves contain high frequency components, a broadband energy distribution, approximately from 10 Hz to 500 Hz, can be observed in k-space [Fig. 4(c)]. In Fig. 4(b), a narrowband energy distribution, approximate from 10 to 100 Hz, comes from low frequency components in longer waves.

Twenty cases of capillary waves were collected to calculate mean C_{pCap_deep} with standard deviations (SDs) from dispersion curves [Fig. 4(d)]. The mean C_{pCap_deep} with SDs for shorter waves was 0.45 ± 0.0148 m/s and 0.37 ± 0.0146 m/s for longer waves, based on the frequency range of 100 Hz to 400 Hz. In theoretical calculations, we selected a 70% bandwidth centered at the peak of the magnitude distribution in k-space, which corresponded with wavenumbers k from 20 to 250 1/m in longer waves [yellow arrow on the Fig. 4(b)] and from 200 to 700 1/m in shorter

Biomedical Optics EXPRESS

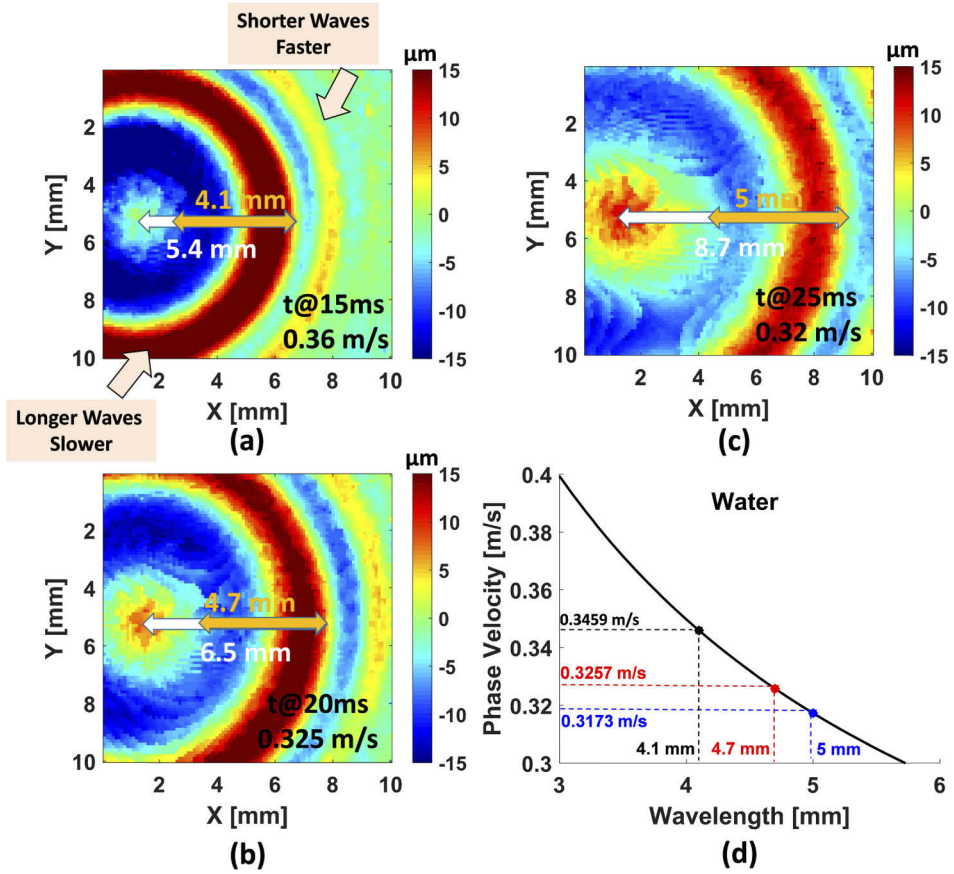

Fig. 3. An example of a 3D-OCT wave motion image to display capillary waves on water. The colorbars indicate surface displacement amplitude. The (a-c) at different time points clearly shown that the shorter wave goes faster and the longer wave is behind the shorter waves. The white arrow and orange arrow in (a-c) indicated the wavefront of the longer waves and wavelengths, respectively. (d) The theoretical results of phase velocities of the capillary waves based on the wavelengths measured from (a-c).

waves [yellow arrow on the Fig. 4(c)] for Eq. (5). In our experiments, the 70% bandwidth was chosen as a reasonable range for wavenumbers in capillary regimes. If wavenumbers are very large, waves enter capillary-gravity regimes; on the contrary, waves will be in gravity regimes once wavenumbers are too small. In theory, the mean C_{pCap_deep} with SDs were 0.45 ± 0.073 m/s in shorter waves and 0.26 ± 0.035 m/s in longer waves. Our experimental results were highly comparable with theoretical calculations in shorter waves due to small change of wavelengths. The reason that phase velocities in longer waves decreased to 0.26 m/s, which is slightly lower than our experimental results, is because larger wavelengths were considered in theory to be gravity waves in shallow water regime, $C_{pGra\_shallow}$ (larger than critical wavelength). In this regime, there is no dispersion and wavelengths travel at the same speed [blue line in Fig. 4(e)] [43]. Therefore, phase velocities were dominated by gravity waves in shallow water, 0.23 m/s. If we checked the wavelength at 4 mm (smaller than critical wavelength), the phase velocity, in longer waves, was 0.35 m/s [Fig. 4(e)] as the comparable result with our experimental result (0.37 ± 0.0146 m/s).

Biomedical Optics EXPRESS

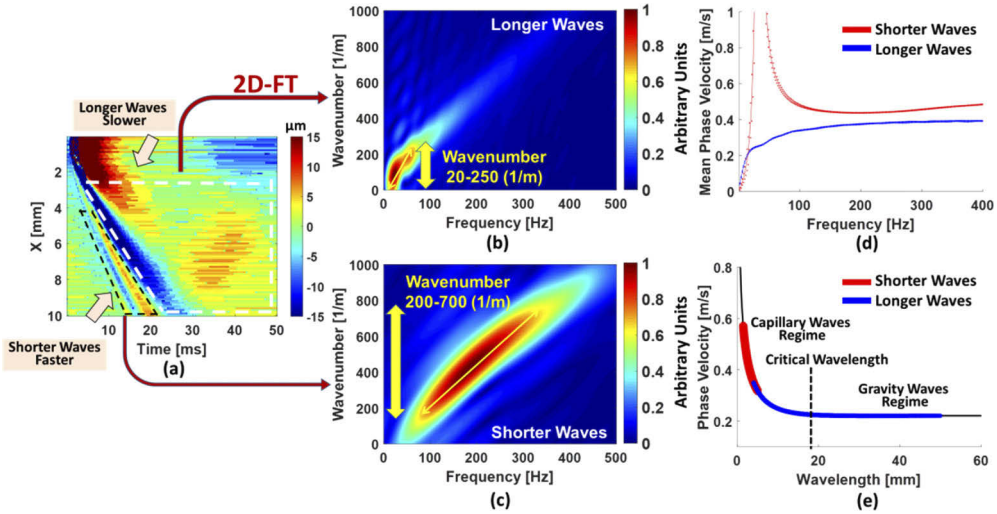

Fig. 4. An example illustrates the phase velocity of capillary waves in water. (a) A 2D-OCT displacement image. The shorter waves (black dashed quadrilateral) and longer waves (white dashed quadrilateral) were clearly observed and it is shown that shorter waves were faster than longer waves. The *k*-space of longer waves and shorter waves were displayed in (b) and (c), respectively. The wavenumber range was selected with a 70% bandwidth centered at the peak of the magnitude distribution (yellow arrow). (d) The mean dispersion curves with the standard deviation of shorter waves (red line) and longer waves (blue line) were presented as the experimental results. (e) The theoretical results of shorter waves and longer waves were illustrated, based on the ranges of wavenumbers indicated in (b) and (c). The colorbar in (a) indicate surface displacement.

The capillary waves in porcine whole blood and plasma were also investigated. The capillary waves were recorded by OCT and twenty cases were collected for each sample. Figure 5(a) and 5(c) are examples of a 2D wave motion image in whole blood and plasma, and Fig. 5(b) and 5(d) are examples of a *k*-space calculated by performing 2D-FT to the white dashed region on the Fig. 5(a) and 5(b). An approximate 70% range about the peak of the magnitude distribution in *k*-space was also selected for comparison with the theoretical calculations. The wavenumber ranges 60-200 1/m for whole blood and 40-190 1/m for plasma. The mean phase velocity, from the dispersion curves in Fig. 5(e), at the range of frequencies between 20 and 100 Hz was 0.24 ± 0.0154 m/s in whole blood and 0.26 ± 0.0173 m/s in plasma. In the theoretical calculations, the mean C_{pCap} of whole blood and plasma were 0.22 ± 0.028 m/s and 0.25 ± 0.036 m/s, respectively. The theoretical results were highly comparable with our experimental results but it was slightly high in whole blood due to portion of the phase velocity in the gravity wave regime as indicated in Fig. 5(f). We checked the phase velocity at a single wavelength, such as 10 mm [green dashed line on Fig. 5(f)], the mean phase velocity based on the theory was 0.2 m/s in whole blood, and 0.225 m/s in plasma. Then we examined experimental results with the mean phase velocity from the dispersion curves [Fig. 5(e)] at approximately 20 Hz [green dashed line on Fig. 5(e)], to obtain 0.208 ± 0.001 m/s in whole blood and 0.228 ± 0.002 m/s in plasma. The results from our experiments were highly comparable with the theoretical results. It should be noted that the shorter waves were difficult to observe in whole blood and plasma due to faster attenuation in viscous fluids [54].

In our experiments, both phase velocities in whole blood and in plasma were slightly slower than in water, which is reasonable due to viscous properties of fluids [54,55]. On the other hand, selecting a suitable ROI on the 2D-OCT displacement images [Figs. 4(a), 5(a), 5(c)] and a

Biomedical Optics EXPRESS

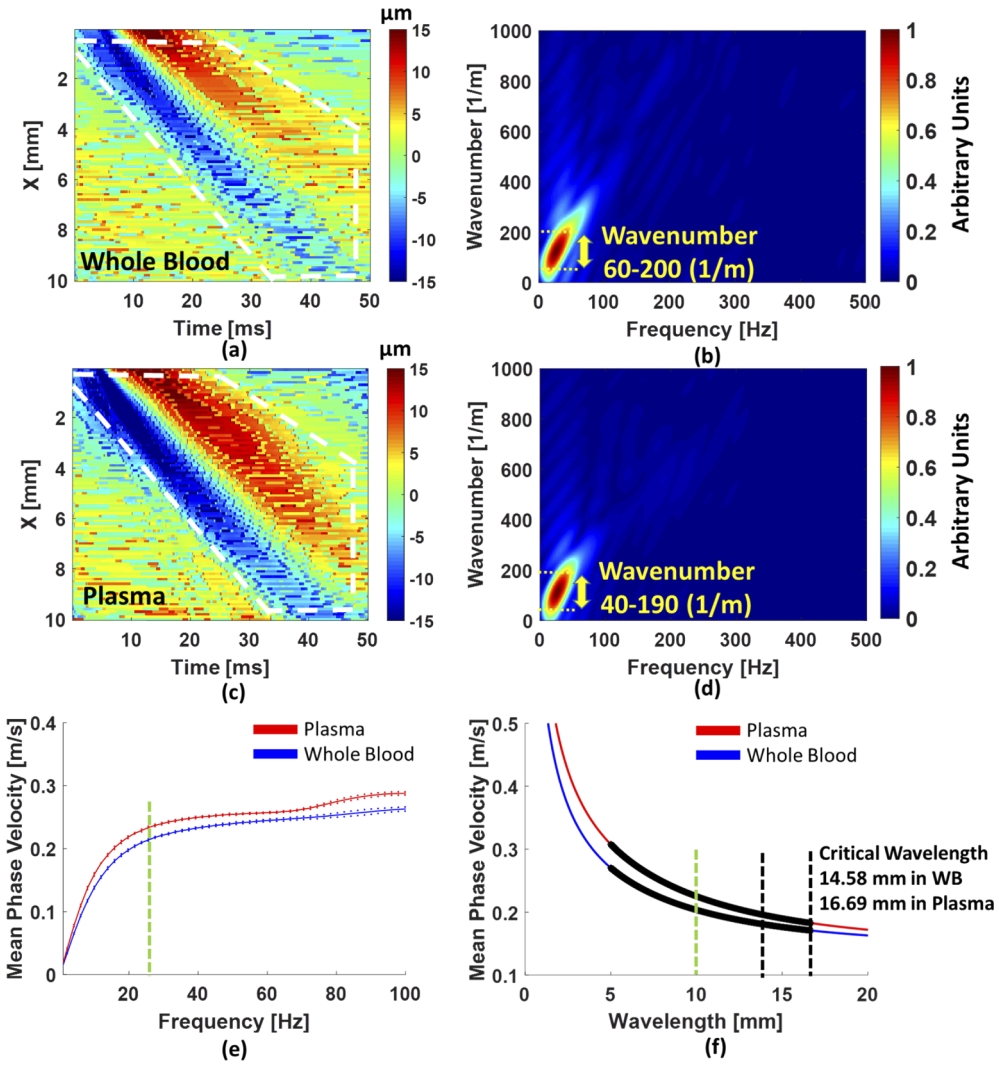

Fig. 5. The phase velocities of capillary waves in whole blood and plasma were exhibited. (a) and (c) are the 2D-OCT lateral time to peak displacement image in whole blood and in plasma, respectively. The longer waves (white dashed quadrilateral) in whole blood and plasma were clearly observed. (b) and (d) The *k*-space of longer waves in whole blood and in plasma were displayed and the wavenumber range was 70% centered at the peak of the magnitude distribution (yellow arrow). (e) The mean dispersion curves with standard deviations in plasma (red line) and whole blood (blue line) were presented as the experimental results. (f) The phase velocities from the theory in plasma and whole blood were represented. The wavelengths were selected by the range of wavenumbers in (b) and (d). The colorbars in (a) and (c) indicate surface displacement.

Biomedical Optics EXPRESS

range in k-space might need special attention. Keeping the same ROIs for each case can provide results with consistency. Furthermore, it might be wrong to evaluate wave speeds from Figs. 4(a), 5(a) and 5(c) by calculating the slope of blue beams because phase velocities of capillary waves in fluids are a function of the wavelength [Eqs. (12)–(14)]. Therefore, a reliable way to evaluate phase velocities in fluids is to transfer wave motions into k-space. We should also note that the precision of the measurement is related to the spatial sampling and the FFT grid sizes that were used. In the study, we reported that OCT would be a promising tool to evaluate the phase velocities of capillary waves on the air-whole blood and air-plasma interfacial surfaces. Also, the results indicated that the mean C_{pCap} is faster in plasma than in whole blood which were presented in both dispersion curves [Fig. 5(c)] and theoretical results [Fig. 5(d)] with good agreement.

In Fig. 3, the precision of our measurement of wavelength was limited by the 0.1 mm spatial sampling. Due to the nonlinear curve in Fig. 3(d), the precision of the speed variation would vary versus wavelength. Our fundamental measurement in this paper is from the 2D Fourier transform analysis so the precision or sensitivity will be governed by the sampling of the k-space. When computing the 2D Fourier transform we used a computation grid size of 5120×5120, which yielded $\Delta k = 1.96$ 1/m and $\Delta f = 0.391$ Hz. We calculated the phase velocities with Δk from 1 Hz to 400 Hz in water and from 1 Hz to 100 Hz in whole blood and plasma to demonstrate how much the dispersion curves would change. The capillary wave phase velocity changes with precision of 0.0013 m/s based on the frequency range of 100 Hz to 400 Hz in water. At the range of frequencies between 20 and 100 Hz, the mean phase velocity changes with precision of 0.0023m/s in whole blood and 0.0025 m/s in plasma. On the other hand, assuming the theoretical calculation in the manuscript as the ground truth, the accuracy of mean phase velocity is 94.59% in water, 91.66% in whole blood and 96.15% in plasma.

It is well known that viscosity disorders of blood and plasma in clinics are mainly associated with various diseases such as hyperviscosity syndromes, stroke or cardiovascular problems [6,11,12,56,57] and fluid viscosities and surface tension can be determined by capillary waves [1,43,54]. According to Stokes theory, the viscosity can be determined by the attenuation of capillary waves. The relationship between viscosities μ and capillary velocity can be expressed as

$$\mu = \frac{\alpha\rho}{2k^2} Cg \tag{16}$$

where α is attenuation coefficient and can be given by

$$\alpha = \frac{\ln\left(\frac{a_1}{a_2}\right)}{x_2 - x_1} \tag{17}$$

where a is wave amplitude and x is the location along the propagation path from the source. The subscripts 1 and 2 are related to the different locations and the associated amplitudes at those locations [1,58]. The proposed technique is fundamental for future potential applications to evaluate viscosities and surface tension in various biological fluids based on capillary waves.

4. Conclusion

We reported that phase velocities of capillary waves in water, porcine whole blood and plasma were evaluated by OCT. The shorter wave and longer waves on water were clearly observed by 3D-OCT images. The theoretical calculations for phase velocities were highly comparable with our experimental results. The phase velocities of capillary waves in water were faster than in porcine whole blood and plasma, and the phase velocity of capillary waves in plasma was faster than in porcine whole blood. These experimental results were in good agreement with theoretical calculations for blood and plasma. The estimation of surface tension and viscosities of fluids will be explored using OCT with capillary waves in future studies.

Biomedical Optics EXPRESS

Funding

National Institutes of Health (R01 DK092255).

Acknowledgments

The content is solely the responsibility of authors and does not necessarily represent the official views of the National Institute of Diabetes and Digestive and Kidney Diseases or the National Institutes of Health. The authors thank Jennifer L. Poston for administrative assistance.

Disclosures

The authors declare that there are no conflicts of interest related to this article.

References

1. F. Behroozi, J. Smith, and W. Even, "Stokes' dream: Measurement of fluid viscosity from the attenuation of capillary waves," Am. J. Phys. **78**(11), 1165–1169 (2010).
2. E. Hrncir and J. Rosina, "Surface tension of blood," Physiol. Res. **46**(4), 319–321 (1997).
3. G. W. Tietjen, S. Chien, E. C. Leroy, I. Gavras, H. Gavras, and F. E. Gump, "Blood viscosity, plasma proteins, and Raynaud syndrome," Arch. Surg. **110**(11), 1343–1346 (1975).
4. L. Campo-Deano, R. P. A. Dullens, D. G. A. L. Aarts, F. T. Pinho, and M. S. N. Oliveira, "Viscoelasticity of blood and viscoelastic blood analogues for use in polydymethylsiloxane in vitro models of the circulatory system," Biomicrofluidics **7**(3), 034102 (2013).
5. O. Linderkamp, H. T. Versmold, K. P. Riegel, and K. Betke, "Contributions of Red-Cells and Plasma to Blood-Viscosity in Preterm and Full-Term Infants and Adults," Pediatrics **74**(1), 45–51 (1984).
6. T. Somer and H. J. Meiselman, "Disorders of blood viscosity," Ann. Med. **25**(1), 31–39 (1993).
7. L. Dintenfass, "Blood rheology as a factor in the pathogenesis of coronary heart disease," Isr. J. Med. Sci. **5**(4), 652–656 (1969).
8. L. Dintenfass, "Blood rheology in pathogenesis of the coronary heart diseases," Am. Heart J. **77**(1), 139–147 (1969).
9. G. Kesmarky, P. Kenyeres, M. Rabai, and K. Toth, "Plasma viscosity: a forgotten variable," Clin. Hemorheol. Microcirc. **39**(1–4), 243–246 (2008).
10. E. Ernst, K. L. Resch, A. Matrai, M. Buhl, P. Schlosser, and H. F. Paulsen, "Impaired blood rheology: a risk factor after stroke?" J. Intern. Med. **229**(5), 457–462 (1991).
11. R. C. Williams Jr., "Hyperviscosity syndromes," Circulation **38**(3), 450–452 (1968).
12. R. Wells, "Syndromes of hyperviscosity," N. Engl. J. Med. **283**(4), 183–186 (1970).
13. J. L. Fahey, W. F. Barth, and A. Solomon, "Serum Hyperviscosity Syndrome," JAMA **192**(6), 464–467 (1965).
14. D. Whiting and J. A. DiNardo, "TEG and ROTEM: Technology and clinical applications," Am. J. Hematol. **89**(2), 228–232 (2014).
15. A. Chen and J. Teruya, "Global hemostasis testing thromboelastography: old technology, new applications," Clin. Lab. Med. **29**(2), 391–407 (2009).
16. X. Xu, J. Zhu, and Z. Chen, "Dynamic and quantitative assessment of blood coagulation using optical coherence elastography," Sci. Rep. **6**(1), 24294 (2016).
17. R. Khnouf, D. Karasneh, E. Abdulhay, A. Abdelhay, W. Sheng, and Z. H. Fan, "Microfluidics-based device for the measurement of blood viscosity and its modeling based on shear rate, temperature, and heparin concentration," Biomed. Microdevices **21**(4), 80 (2019).
18. Y. Jun Kang, E. Yeom, and S. J. Lee, "A microfluidic device for simultaneous measurement of viscosity and flow rate of blood in a complex fluidic network," Biomicrofluidics **7**(5), 054111 (2013).
19. D. Mark, S. Haeberle, G. Roth, F. von Stetten, and R. Zengerle, "Microfluidic lab-on-a-chip platforms: requirements, characteristics and applications," Chem. Soc. Rev. **39**(3), 1153–1182 (2010).
20. D. T. Chiu, A. J. deMello, D. Di Carlo, P. S. Doyle, C. Hansen, R. M. Maceiczyk, and R. C. R. Wootton, "Small but Perfectly Formed? Successes, Challenges, and Opportunities for Microfluidics in the Chemical and Biological Sciences," Chem **2**(2), 201–223 (2017).
21. K. S. Yemul, A. M. Zysk, A. L. Richardson, K. V. Tangella, and L. K. Jacobs, "Interpretation of Optical Coherence Tomography Images for Breast Tissue Assessment," Surg. Innov. **26**(1), 50–56 (2019).
22. K. V. Larin and D. D. Sampson, "Optical coherence elastography - OCT at work in tissue biomechanics [Invited]," Biomed. Opt. Express **8**(2), 1172–1202 (2017).
23. Y. Qiu, Y. Wang, Y. Xu, N. Chandra, J. Haorah, B. Hubbi, B. J. Pfister, and X. Liu, "Quantitative optical coherence elastography based on fiber-optic probe for in situ measurement of tissue mechanical properties," Biomed. Opt. Express **7**(2), 688–700 (2016).
24. S. Wang and K. V. Larin, "Optical coherence elastography for tissue characterization: a review," J. Biophotonics **8**(4), 279–302 (2015).

Biomedical Optics EXPRESS

25. C. Sun, B. Standish, and V. X. Yang, "Optical coherence elastography: current status and future applications," J. Biomed. Opt. **16**(4), 043001 (2011).
26. M. Razani, A. Mariampillai, C. R. Sun, T. W. H. Luk, V. X. D. Yang, and M. C. Kolios, "Feasibility of optical coherence elastography measurements of shear wave propagation in homogeneous tissue equivalent phantoms," Biomed. Opt. Express **3**(5), 972–980 (2012).
27. C. H. Li, G. Y. Guan, R. Reif, Z. H. Huang, and R. K. K. Wang, "Determining elastic properties of skin by measuring surface waves from an impulse mechanical stimulus using phase-sensitive optical coherence tomography," J. R. Soc. Interface **9**(70), 831–841 (2012).
28. C. H. Li, G. Y. Guan, S. A. Li, Z. H. Huang, and R. K. Wang, "Evaluating elastic properties of heterogeneous soft tissue by surface acoustic waves detected by phase-sensitive optical coherence tomography," J. Biomed. Opt. **17**(5), 057002 (2012).
29. X. Liang, S. G. Adie, R. John, and S. A. Boppart, "Dynamic spectral-domain optical coherence elastography for tissue characterization," Opt. Express **18**(13), 14183–14190 (2010).
30. C. H. Li, G. Y. Guan, Y. T. Ling, Y. T. Hsu, S. Z. Song, J. T. J. Huang, S. Lang, R. K. K. Wang, Z. H. Huang, and G. Nabi, "Detection and characterisation of biopsy tissue using quantitative optical coherence elastography (OCE) in men with suspected prostate cancer," Cancer Lett. **357**(1), 121–128 (2015).
31. M. Razani, T. W. Luk, A. Mariampillai, P. Siegler, T. R. Kiehl, M. C. Kolios, and V. X. Yang, "Optical coherence tomography detection of shear wave propagation in inhomogeneous tissue equivalent phantoms and ex-vivo carotid artery samples," Biomed. Opt. Express **5**(3), 895–906 (2014).
32. M. A. Kirby, I. Pelivanov, S. Song, L. Ambrozinski, S. J. Yoon, L. Gao, D. Li, T. T. Shen, R. K. Wang, and M. O'Donnell, "Optical coherence elastography in ophthalmology," J. Biomed. Opt. **22**(12), 1–28 (2017).
33. L. Ambrozinski, S. Z. Song, S. J. Yoon, I. Pelivanov, D. Li, L. Gao, T. T. Shen, R. K. K. Wang, and M. O'Donnell, "Acoustic micro-tapping for non-contact 4D imaging of tissue elasticity," Sci Rep-Uk **6**(1), 38967 (2016).
34. R. K. Manapuram, S. A. Baranov, V. G. R. Manne, N. Sudheendran, M. Mashiatulla, S. Aglyamov, S. Emelianov, and K. V. Larin, "Assessment of wave propagation on surfaces of crystalline lens with phase sensitive optical coherence tomography," Laser Phys. Lett. **8**(2), 164–168 (2011).
35. Z. L. Han, S. R. Aglyamov, J. S. Li, M. Singh, S. Wang, S. Vantipalli, C. Wu, C. H. Liu, M. D. Twa, and K. V. Larin, "Quantitative assessment of corneal viscoelasticity using optical coherence elastography and a modified Rayleigh-Lamb equation," J. Biomed. Opt. **20**(2), 020501 (2015).
36. Z. L. Han, J. S. Li, M. Singh, C. Wu, C. H. Liu, R. Raghunathan, S. R. Aglyamov, S. Vantipalli, M. D. Twa, and K. V. Larin, "Optical coherence elastography assessment of corneal viscoelasticity with a modified Rayleigh-Lamb wave model," J. Mech. Behav. Biomed. **66**, 87–94 (2017).
37. S. Wang and K. V. Larin, "Shear wave imaging optical coherence tomography (SWI-OCT) for ocular tissue biomechanics," Opt. Lett. **39**(1), 41–44 (2014).
38. S. Song, N. M. Le, Z. Huang, T. Shen, and R. K. Wang, "Quantitative shear-wave optical coherence elastography with a programmable phased array ultrasound as the wave source," Opt. Lett. **40**(21), 5007–5010 (2015).
39. A. Nahas, M. Tanter, T. M. Nguyen, J. M. Chassot, M. Fink, and A. Claude Boccara, "From supersonic shear wave imaging to full-field optical coherence shear wave elastography," J. Biomed. Opt. **18**(12), 121514 (2013).
40. A. L. Oldenburg, G. Wu, D. Spivak, F. Tsui, A. S. Wolberg, and T. H. Fischer, "Imaging and Elastometry of Blood Clots Using Magnetomotive Optical Coherence Tomography and Labeled Platelets," IEEE J. Sel. Top. Quantum Electron. **18**(3), 1100–1109 (2012).
41. M. M. Tripathi, Z. Hajjarian, E. M. Van Cott, and S. K. Nadkarni, "Assessing blood coagulation status with laser speckle rheology," Biomed. Opt. Express **5**(3), 817–831 (2014).
42. Y. V. Sanochkin, "Viscosity effect on free surface waves in fluids," Fluid Dyn. **35**(4), 599–604 (2000).
43. H. Lamb, *Hydrodynamics* (Cambridge University Press, 1932).
44. S. Song, Z. Huang, and R. K. Wang, "Tracking mechanical wave propagation within tissue using phase-sensitive optical coherence tomography: motion artifact and its compensation," J. Biomed. Opt. **18**(12), 121505 (2013).
45. K. K. Shung, "Diagnostic ultrasound : imaging and blood flow measurements," (2015).
46. M. W. Urban, M. Fatemi, and J. F. Greenleaf, "Modulation of ultrasound to produce multifrequency radiation force," J. Acoust. Soc. Am. **127**(3), 1228–1238 (2010).
47. K. A. Rosentrater and R. A. Flores, "Physical and rheological properties of slaughterhouse swine blood and blood components," Trans. ASAE **40**(3), 683–689 (1997).
48. D. J. Vitello, R. M. Ripper, M. R. Fettiplace, G. L. Weinberg, and J. M. Vitello, "Blood Density Is Nearly Equal to Water Density: A Validation Study of the Gravimetric Method of Measuring Intraoperative Blood Loss," J. Vet. Med. **2015**, 1–4 (2015).
49. R. J. Trudnowski and R. C. Rico, "Specific gravity of blood and plasma at 4 and 37 degrees C," Clin. Chem. **20**(5), 615–616 (1974).
50. S. Zaitsev, "Dynamic surface tension measurements as general approach to the analysis of animal blood plasma and serum," Adv. Colloid Interface Sci. **235**, 201–213 (2016).
51. M. L. Palmeri, M. H. Wang, J. J. Dahl, K. D. Frinkley, and K. R. Nightingale, "Quantifying hepatic shear modulus in vivo using acoustic radiation force," Ultrasound Med Biol. **34**(4), 546–558 (2008).
52. H. C. Liu, P. Kijanka, and M. W. Urban, "Acoustic radiation force optical coherence elastography for evaluating mechanical properties of soft condensed matters and its biological applications," *J Biophotonics* e201960134 (2019).

Biomedical Optics EXPRESS

53. M. Bernal, I. Nenadic, M. W. Urban, and J. F. Greenleaf, "Material property estimation for tubes and arteries using ultrasound radiation force and analysis of propagating modes," J. Acoust. Soc. Am. **129**(3), 1344–1354 (2011).
54. F. Behroozi, J. Smith, and W. Even, "Effect of viscosity on dispersion of capillary-gravity waves," Wave Motion **48**(2), 176–183 (2011).
55. S. Neogi, A. Lee, and W. P. Jepson, "A Model for Multiphase (Gas-Water-Oil) Stratified Flow in Horizontal Pipelines," in *SPE Asia Pacific Oil and Gas Conference*, (Society of Petroleum Engineers, Melbourne, Australia, 1994), p. 10.
56. E. Fukada, "Measurement of blood viscosity with respect to clinical diagnosis," Ann. N Y Acad. Sci. **130**(3), 920–924 (1966).
57. J. Harkness, "The viscosity of human blood plasma; its measurement in health and disease," Biorheology **8**(3-4), 171–193 (1971).
58. F. Behroozi, "Fluid viscosity and the attenuation of surface waves: a derivation based on conservation of energy," Eur. J. Phys. **25**(1), 115–122 (2004).